

Ionization balance of Ti in the photospheres of the Sun and four late-type stars

Maria Bergemann^{*}

Max-Planck Institute for Astrophysics, Karl-Schwarzschild Str. 1, 85741, Garching, Germany

Accepted Date. Received Date; in original Date

ABSTRACT

In this paper we investigate statistical equilibrium of Ti in the atmospheres of late-type stars. The Ti I/Ti II level populations are computed with available experimental atomic data, except for photoionization and collision induced transition rates, for which we have to rely on theoretical approximations. For the Sun, the NLTE line formation with adjusted H I inelastic collision rates and MAFAGS-OS model atmosphere solve the long-standing discrepancy between Ti I and Ti II lines. The NLTE abundances determined from both ionization stages agree within 0.01 dex with each other and with the Ti abundance in C I meteorites. The Ti NLTE model does not perform similarly well for the metal-poor stars, overestimating NLTE effects in the atmospheres of dwarfs, but underestimating overionization for giants. Investigating different sources of errors, we find that only [Ti/Fe] ratios based on Ti II and Fe II lines can be safely used in studies of Galactic chemical evolution. To avoid spurious abundance trends with metallicity and dwarf/giant discrepancies, it is strongly recommended to disregard Ti I lines in abundance analyses, as well as in determination of surface gravities.

Key words: Radiative transfer – Line: profiles – Line: formation – Sun: abundances – Stars: abundances

1 INTRODUCTION

Most of abundance analyses in metal-poor stars focus on few key elements, among others, Ti. This has several reasons. The main nucleosynthesis site of Ti has not yet been unambiguously identified and all models of Galactic chemical evolution completely fail to describe observational trend of [Ti/Fe] with metallicity (McWilliam et al. 1995), which increases with decreasing [Fe/H]. In spectra of late-type stars, Ti is represented by a large number of spectral lines in both neutral and ionized stages. Therefore, Ti can be used to verify basic stellar parameters (T_{eff} , $\log g$) and microturbulence, which are determined, for example, by means of photometric methods or from the excitation and ionization balance of Fe¹.

Traditionally, Ti abundances in stellar atmospheres are determined assuming that distributions of atoms among excitation states and ionization stages derive from the formulas of Saha-Boltzmann for the local values of electron temperature and density in models of atmospheres, so-called local thermodynamic equilibrium (LTE). Important evidence against this assumption comes, in

return, from LTE analyses of high-resolution spectra. It is known that low-excitation Ti I lines deliver systematically lower abundances compared to the high-excitation lines and lines of Ti II for different stellar parameters. LTE studies of the Sun with 1D static (Blackwell et al. 1987) and 3D hydrodynamical model atmospheres (Asplund et al. 2009) demonstrate that these discrepancies are larger than 0.1 dex, which is unacceptable given the precisely known fundamental parameters of the Sun. The same problem was reported for other nearby stars with well-known parameters, such as Pollux (Ruland et al. 1980).

Analyses of metal-poor stars also point to pronounced NLTE effects on Ti I in their atmospheres. Systematically higher [Ti/Fe] abundance ratios in metal-poor dwarfs compared to giants with similar metallicities were reported by Bonifacio et al. (2009). Positive offsets between abundances based on Ti II and Ti I lines were reported for horizontal branch stars (Clementini et al. 1995) and for giants (Brown et al. 1983; Gratton & Sneden 1991; Johnson 2002; Tafelmeyer et al. 2010). Lai et al. (2008) found a trend of [Ti/Fe] abundances ratios with stellar T_{eff} , which was supported by the data of Preston et al. (2006), Cayrel et al. (2004), and Cohen et al. (2004).

Theoretical studies of NLTE effects in Ti are very sparse. Hauschildt, Allard & Baron (1999) investigated statistical equilibrium of Ti in M-type dwarfs and giants. They found small effect of Ti I overionization on the number density of TiO molecules, the main opacity agent in the atmospheres of M stars. However,

^{*} E-mail: mbergema@mpa-garching.mpg.de

¹ In this context the notation of excitation and ionization equilibrium refers to the equality of abundances determined from all detected spectral lines of an element, which is represented by several ionization stages in a stellar atmosphere

they demonstrated that the NLTE effects on the Ti I line formation are important and grow with increasing model T_{eff} for dwarfs and decreasing T_{eff} for giants. Manso Sainz & Landi Degl'Innocenti (2002) and Shchukina & Trujillo Bueno (2009) used NLTE populations of Ti to model polarization in the Ti I lines of multiplet 42. Their goal was to study weak solar magnetic fields. None of the investigations focused on the NLTE effects on Ti abundances in stellar atmospheres.

We present first results of a study aimed at the NLTE modelling of Ti line formation in the atmospheres of late-type stars. In Sect. 2, we give a detailed description of the methods developed for NLTE and spectrum synthesis calculations. Statistical equilibrium of Ti for a restricted range of stellar parameters is discussed in Sect. 3.1. Ti abundances for the Sun and four metal-poor stars are given in Sect. 3. The results are summarized in Sect. 4.

2 METHODS

In order to carry out the abundance analysis, we use a unique program package developed at the University Observatory Munich (the group of T. Gehren). The package consists of three codes, which have been developed consistently and are adapted for spectroscopic analysis of A-, F- and G-type stars. MAFAGS is a 1D LTE model atmosphere code. Detail is a code for solving multi-level non-LTE radiative transfer problems with a *given* static 1D model atmosphere. SIU is an interactive non-LTE spectrum synthesis code that makes use of MAFAGS model atmospheres and level populations from DETAIL. Below, we give some details for each of the programs. The general procedure of abundance determination is the same as in our previous work on Mn, Co, and Cr (Bergemann & Gehren 2008; Bergemann, Pickering & Gehren 2010; Bergemann & Cescutti 2010).

2.1 Model atmospheres

The static plane-parallel LTE model atmospheres were kindly generated by F. Grupp with the MAFAGS code. In the most recent version, MAFAGS-OS, line blanketing is treated with an opacity sampling method, with line absorption sampled at $\sim 86\,000$ wavelength points. All opacity sources relevant to modelling A0-K0 stars including line absorption due to various diatomic molecules are taken into account. Full description of these models, including the reference set of solar element abundances, as well as selection criteria of the wavelength grid and lines, is given in Grupp (2004a). In particular, $\log \epsilon_{\text{Fe}} = 7.50$ was adopted, which is consistent with the NLTE solar abundance of Fe determined by Gehren et al. (2001). Convection is included in the formulation of Canuto & Mazzitelli (1991), which differs from the mixing-length theory of Böhm-Vitense (1958) in that it assumes a full spectrum of turbulent eddies. Compressible turbulence is accounted for using the mixing length, $\Lambda = \alpha_{\text{cm}}/H_p$, where H_p is the pressure scale height and the free parameter α_{cm} is set to 0.82. The latter value was derived by Bernkopf (1998) from stellar evolution calculations for the Sun and from the requirement that the MAFAGS models fit the observed Balmer line profiles.

We also performed abundance calculations with the model atmospheres computed with older version of the MAFAGS code (Fuhrmann et al. 1997); these models were used to determine spectroscopic stellar parameters for the selected stars (Sect. 3.3.2). This version is based on opacity distribution functions (ODF) from

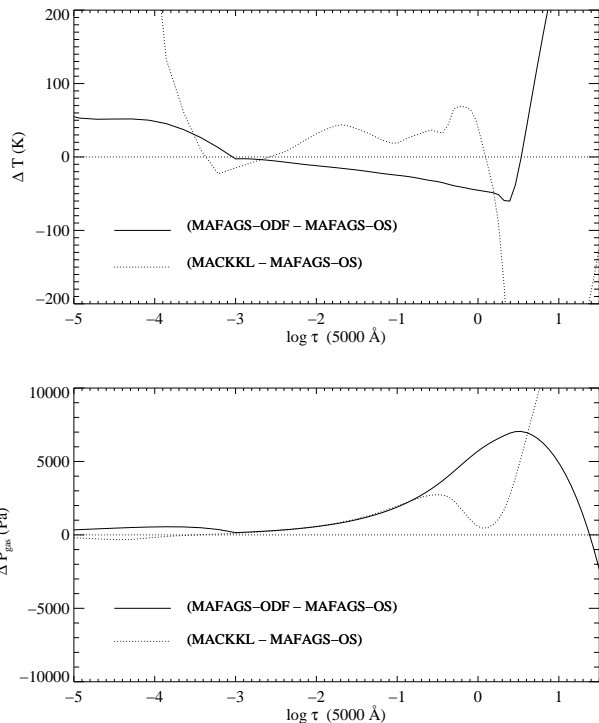


Figure 1. Difference in temperature and gas pressure stratifications of the solar theoretical MAFAGS-OS, MAFAGS-ODF, and semi-empirical MACKKL models.

Kurucz (1992). Convection was taken into account with the mixing-length theory (Böhm-Vitense 1958) and the mixing length was set to 0.5 pressure scale heights, the latter value was also calibrated on the solar Balmer lines by Fuhrmann, Axer & Gehren (1993). A detailed comparison of the solar MAFAGS-ODF and MAFAGS-OS models is given in Grupp (2004b).

MAFAGS models do not include chromospheres that is the case with all other theoretical 1D models so far. Clearly, this is a crude approximation for the Sun. The existence of chromospheres has also been demonstrated for metal-poor dwarfs (Smith & Churchill 1998) and giants (Dupree, Hartmann & Smith 1990). To discuss this deficiency of the models, we will also present some results for the semi-empirical solar model atmosphere with chromosphere (Maltby et al. 1986, hereafter MACKKL). The MACKKL model was interpolated to 80 depth points to increase numerical accuracy in line formation calculations (Reetz 1999, PhD thesis). Differences between temperature and pressure stratifications of the solar MACKKL, MAFAGS-ODF, and MAFAGS-OS models as a function of continuum optical depth at 5000 \AA , $\log \tau_{5000}$, are shown in Fig. 1.

We emphasize that the semi-empirical model atmosphere is used here only to demonstrate the shortcomings of the theoretical atmospheres, which are still the main tool to model any star other than the Sun. Thus, the solar abundance analysis, as well as the differential analysis of the metal-poor stars, are performed only with the MAFAGS models.

2.2 Statistical equilibrium and line formation codes

The NLTE level populations for Ti were computed with an updated version of the DETAIL code (Butler & Giddings 1985). In calcula-

tions of statistical equilibrium, each Ti line was treated with a Gaussian profile with 9 frequency points. The code solves a restricted NLTE problem, i.e. coupled statistical equilibrium and radiative transfer equations are solved for a fixed input model atmosphere. This may not be a bad approximation for Ti in the range of stellar parameters we are interested in. Ti I, which is, in fact, affected by NLTE, is not an important opacity source in the atmospheres of FG stars and does not contribute significantly to the free electron pool due to the low element abundance. Ti II is the dominant ionization stage and its number densities are well described in LTE (see Sect. 3.1). Hauschildt et al. (1999) computed full NLTE line-blanketed model atmospheres for M dwarfs and giants with solar metallicity including Ti as one of the NLTE species. They showed that the NLTE effects in Ti influence the atmospheres of cool stars only in the upper layers by changing the concentration of TiO^+ molecules, and the effect on the number density of TiO molecules is negligible. Also, the effect of Ti on the atmospheric structure, even if present, is much smaller than that of Fe, which is an important source of the bound-free opacity in the UV and has, by far, the largest number of lines all over the spectrum of a typical F-type star (Grupp et al. 2009, Fig. 1).

Still one has to keep in mind that, in general, the assumption of LTE in modelling stellar atmospheres is not realistic. As demonstrated by Short & Hauschildt (2005), the *integral* effect of NLTE in Fe-group elements (Ti, Mn, Fe, Co, Ni) on the structure of the solar model atmosphere is significant. The differences in the temperature structure of their NLTE PHOENIX model with respect to LTE models are as large as ± 200 K at different depths. These differences are comparable with the temperature fluctuations in the line forming regions in the 3D hydrodynamical solar model (Asplund 2005). Since NLTE effects in the presence of convective inhomogeneities are amplified (Fe: Shchukina & Trujillo Bueno 2001), one can expect that self-consistent 3D NLTE hydrodynamical model atmospheres will have radically different structure compared to existing 1D LTE, 1D NLTE, or 3D LTE models. On the other side, such physically realistic models do not exist yet, and there is little chance they will appear in the near future.

Emergent flux spectra were computed with an updated version of the code SIU (Reetz 1999), using MAFAGS model atmospheres and departure coefficients of Ti I/Ti II levels from the DETAIL code. Ti lines were computed with full Voigt profiles taking into account various broadening processes (see Sect. 3.2). Ti abundances were determined by visually fitting the LTE and NLTE synthetic line profiles to the observed flux spectra including LTE modelling of blending features. This method is more reliable than χ -square fitting or equivalent width (EW) measurements for the solar-type stars, because a majority of Ti I and Ti II lines are blended and/or display an asymmetry in the core and red wing, which is a typical signature of atmospheric temperature and velocity inhomogeneities (e.g. Asplund et al. 2000) not taken into account by static plane-parallel model atmospheres.

2.3 Ti model atom

A model of the Ti atom was constructed with energy levels, wavelengths of transitions, and transition probabilities from the Kurucz' database², which includes all laboratory data. The number of energy levels is 216 for Ti I and 77 for Ti II, with uppermost excited

levels located at 0.17 eV and 1.1 eV below the respective ionization limits, 6.82 eV and 13.58 eV. The model is closed by the Ti III ground state. The total number of radiatively-allowed transitions is 4671 (3435 Ti I and 1236 Ti II). Fine structure was neglected in the statistical equilibrium calculations, except for the ground state of Ti I a^3F (configuration $1s^22s^22p^63s^23p^63d^24s^2$). Excitation energy of each LS term was computed as a weighted mean of statistical weights and excitation energies of fine structure sub-levels. Also, transitions between fine structure levels were combined, with the total transition probability of each term being the weighted mean of $\log gf$'s of their fine structure components. A Grotrian diagram for Ti I is shown in Fig. 2.

The electron collision cross-sections from states with allowed bound-bound and bound-free transitions were computed with the formulas of van Regemorter (1962) and Seaton (1962), respectively. Electron collision cross-sections from states connected only by forbidden transitions were treated with the formula of Allen (1973). According to Mashonkina (1996) collision rates obtained with these formulas have only an order of magnitude accuracy.

Threshold photoionization cross-sections for the levels y^3P° (3.93 eV), z^3H° (3.96 eV), and v^3F° (4.2 eV) were taken from Yang et al. (2009) and a hydrogenic approximation was assumed for their frequency variation. The cross-sections were measured by resonance ionization mass spectrometry and for the v^3F° levels they are consistent with Hartree-Fock calculations with relativistic corrections (Saloman 1993). For the other levels, even quantum-mechanical calculations are not available, thus the photoionization cross-sections were derived from the hydrogenic approximation (Mihalas 1978). The experimental threshold cross-sections from Yang et al. (2009) are lower than the hydrogenic cross-sections with effective principal quantum numbers by one order of magnitude. For example, the measured values for the v^3F° fine structure levels are 0.6 – 1.2 Mb, whereas the hydrogenic cross-section is roughly 18 Mb.

In many aspects including the atomic structure, our model atom is very similar to that of Hauschildt et al. (1999) with the main difference³ that inelastic collisions with H I atoms are included in our model. The corresponding bound-bound and bound-free rates were computed from the formulas of Drawin (1969) in the version of Steenbock & Holweger (1984).

Since the atomic data are of a low accuracy, we perform calculations of ionization equilibria for several Ti NLTE model atoms, which differ in the efficiency of e^- and H I collisions (Sect. 3.2.3). Thus, for the total e^- collision rates we use the scaling factors $S_e = 0.01, 1, 10$, and for the H I collision rates $S_H = 0.05, 3$. The final adopted values are $S_H = 3$ and $S_e = 1$, which give the smallest abundance scatter in the solar abundance analysis (see Sect. 3.2).

2.4 Line parameters

A careful selection of Ti lines is essential, because ionization equilibrium of Ti in the solar photosphere is used to calibrate the efficiency of inelastic collisions with H I.

Ti I and Ti II lines were selected by the critical inspection of the KPNO atlas of solar fluxes (Kurucz et al. 1984) and of the disk-center intensity spectrum (Brault & Testerman 1972). For Ti I, we rejected all lines that showed obvious blends in the profile, i.e. the contribution of the theoretically computed blend to the total W_λ of

² <http://kurucz.harvard.edu/atoms.html>

³ Hauschildt et al. (1999) also used different photoionization cross-section for the Ti I ground state.

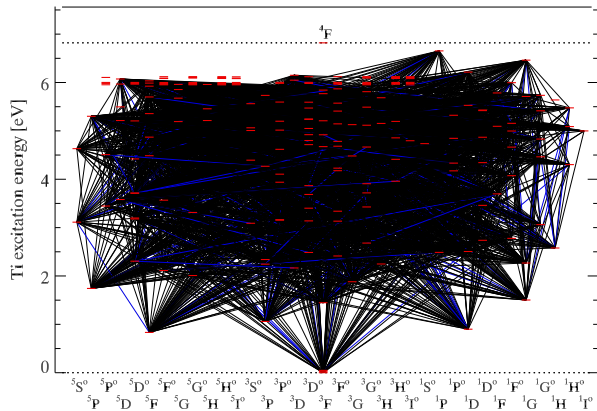


Figure 2. Ti grotian diagram. Strong transitions with $\log gf > -1$ are shown with blue trace.

a line was more than 5 %. For Ti II, this threshold was somewhat higher, because of a very small number of sufficiently strong Ti II lines with reliable transition probabilities.

Some regions in the observed solar spectrum, such as shown in Fig. 3, suffer from excessive line blanketing and are not well reproduced by our model atmospheres and line lists. All Ti lines located in such regions were rejected from the solar analysis. For the other regions, continuum is poorly defined. Following Gehren et al. (2001), we renormalized the continuum in these regions if the depression extended over few tenths of Å. The re-adjustment of the continuum was never larger than $\sim 0.5\%$, which is within the continuum placement uncertainty.

Tables 1 and 2 contain important information for each line including our evaluation of the line ‘quality’ in the solar spectrum, i.e. whether the line is blended or has an asymmetric profile. Term designations, wavelengths and excitation potentials of lower levels were taken from the NIST database, whenever available (otherwise from Martin, Fuhr & Wiese 1988). The equivalent widths given were computed from the best-fitting synthetic profiles, excluding contribution of blends. Equivalent widths are not used in the abundance calculations and serve only as a demonstration of line strength. For example, lines with $W_\lambda < 50$ mÅ are not detectable in our spectra of metal-poor stars.

2.5 Isotopic shift

Ti is represented by five stable isotopes ^{46}Ti : ^{47}Ti : ^{48}Ti : ^{49}Ti : ^{50}Ti and their relative abundances in the solar system are 8 : 7.43 : 73.8 : 5.5 : 5.4⁴, respectively. It has been recognized long ago that Ti lines in the solar spectrum are subject to an additional broadening due to the isotopic effect (Abt 1952). In analogue to hyperfine splitting⁵, isotopic shift of energy levels leads to splitting of spectral lines into several components. For lighter multi-electron atomic systems, such as Ti, the isotopic shift of energy levels is primarily due to the differences in nuclear masses of isotopes giving rise to normal and specific mass shifts. As shown below, non-negligible errors in the

⁴ <http://www.nist.gov/pml/data/handbook/index.cfm>

⁵ Hyperfine splitting also affects atomic energy levels of ^{47}Ti and ^{49}Ti , but the fraction of these odd-Z isotopes is only 13% of the total element abundance. Thus, hyperfine splitting is ignored in this work.

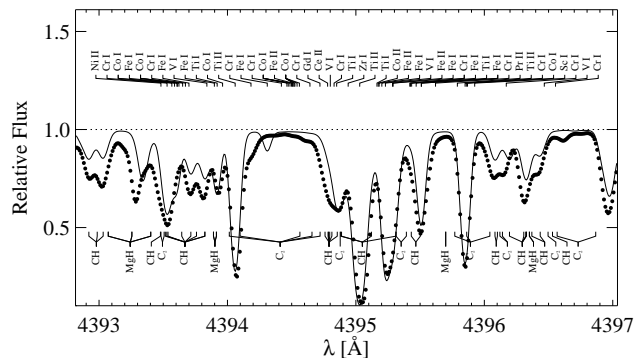


Figure 3. A spectral window in the KPNO atlas of solar fluxes (filled circles) compared to a synthetic spectrum (black trace) computed with the MAFAGS-OS model atmosphere. All lines populating this spectral region are indicated.

solar Ti abundance may arise if isotopic structure is neglected in the line formation calculations.

Isotopic shifts in the UV and blue Ti II transitions were recently calculated by Berengut et al. (2008) and measured by Nouri et al. (2010). For some Ti II transitions, the total separation of components due to the isotopic effect is not larger than $\delta\nu \sim 900$ MHz or $\delta\lambda \sim 6$ mÅ (Nouri et al. 2010). In contrast, very large isotopic shifts have been observed for transitions from the unfilled 3d shell (e.g. $3d^3 4s \rightarrow 3d^2 4p$, or $3d 4s^2 \rightarrow 3d^2 4p$). For the Ti II line at 4488 Å, which we use in our abundance analysis, Nouri et al. (2010) derive an isotope shift of ~ 2400 MHz with the total separation of components of ~ 4500 MHz. This corresponds to a line width of ~ 30 mÅ that is comparable with thermal line broadening in the solar atmosphere. There are also few measurements of the isotopic shift in Ti I, which include several transitions from our sample.

In this study, isotopic structure was taken into account for two Ti I and three Ti II lines, which show large isotopic splittings, i.e. the separation of components is ~ 15 – 20 mÅ. For the Ti I lines, we used the data from Gangrsky, Marinova & Zemlyanoi (1995). The wavelengths and gf -values of individual components are given in Table 3. The total oscillator strengths for the transitions are given in Tables 1 and 2.

3 RESULTS

In the following sections, we present the results of statistical equilibrium calculations for Ti for a restricted range of stellar parameters and discuss whether the LTE approximation can be adopted for different combinations of T_{eff} , $\log g$, and $[\text{Fe}/\text{H}]$. We also compute NLTE abundances of Ti for the Sun and four metal-poor stars (Sect. 3.3.2) and attempt to calibrate the poorly-known cross-sections to inelastic H I and electron collisions following the classical Drawin (1968) formalism to satisfy ionization equilibrium of Ti I/Ti II. Deviations from LTE and their effect on the abundances are discussed in terms of NLTE abundance corrections defined as:

$$\Delta_{\text{NLTE}} = \log \epsilon^{\text{NLTE}} - \log \epsilon^{\text{LTE}}$$

Table 1. Parameters of the Ti I lines used for the spectrum synthesis. The abundances in columns 10–13 are given for gf -values from Blackwell-Whitehead et al. (2006), if the latter are specified in column 7 (otherwise for the gf -values measured by the Oxford group, which are given in column 8, and exact references to the latter are given in column 9).

λ	Mult.	Rem. ^a	Lower level	Upper level	E_{low} [eV]	$\log gf$	$\log gf^b$	Source ^b	W_λ [mÅ]	MAFAGS-ODF		MAFAGS-OS	
										$\log \epsilon_{\text{LTE}}$	$\log \epsilon_{\text{NLTE}}$	$\log \epsilon_{\text{LTE}}$	$\log \epsilon_{\text{NLTE}}$
4281.37	17	b	a^5F_1	$x^5D_2^o$	0.81		-1.303	2	33	4.78	4.81	4.88	4.91
4512.73	16	a	a^5F_4	$y^5F_5^o$	0.84		-0.424	2	67	4.81	4.84	4.92	4.95
4518.03	16	b	a^5F_3	$y^5F_4^o$	0.83		-0.269	2	74	4.82	4.85	4.92	4.95
4533.24	16	b	a^5F_5	$y^5F_5^o$	0.85		0.532	2	113	4.8	4.82	4.89	4.9
4534.78	16	b	a^5F_4	$y^5F_4^o$	0.84		0.336	2	101	4.8	4.82	4.89	4.9
4548.77	16	s	a^5F_3	$y^5F_2^o$	0.83		-0.298	2	73	4.82	4.85	4.92	4.95
4555.49	16	a	a^5F_5	$y^5F_4^o$	0.85		-0.432	2	67	4.82	4.85	4.92	4.95
4562.63	5	b	a^3F_3	$z^1D_2^o$	0.02		-2.600	1	13	4.83	4.87	4.92	4.96
4617.28	57	a	a^5P_3	$w^5D_4^o$	1.75		0.445	4	63	4.75	4.76	4.86	4.87
4639.93	57	b	a^5P_1	$w^5D_1^o$	1.73		-0.136	4	38	4.76	4.79	4.88	4.9
4681.92	4	b	a^3F_4	$z^3G_5^o$	0.05	-1.03	-1.01	1	75	4.8	4.84	4.9	4.94
4758.12	74	b	a^3H_5	$x^3H_5^o$	2.25		0.481	4	46	4.77	4.79	4.86	4.89
4759.27	74	b	a^3H_6	$x^3H_6^o$	2.26		0.570	4	49	4.76	4.78	4.85	4.87
4820.41	55	b	a^1G_4	$y^1F_3^o$	1.50		-0.385	4	44	4.8	4.84	4.88	4.9
4840.88	23	b	a^1D_2	$y^1D_2^o$	0.90		-0.453	2	64	4.82	4.81	4.92	4.93
4964.7	66	b	$z^5G_2^o$	e^5F_2	1.97		-0.819	4	9	4.77	4.8	4.87	4.89
4981.74	13	s	a^5F_5	$y^5G_6^o$	0.85		0.560	2	120	4.78	4.8	4.89	4.91
4991.07	13	b,s	a^5F_4	$y^5G_5^o$	0.84		0.436	2	112	4.78	4.8	4.89	4.91
4997.1	3	a	a^3F_2	$z^3D_2^o$	0.00	-2.07	-2.06	1	34	4.8	4.84	4.9	4.95
4999.51	13	b	a^5F_3	$y^5G_4^o$	0.83		0.306	2	106	4.82	4.85	4.93	4.95
5009.66	3	b,uc	a^3F_3	$z^3D_3^o$	0.02	-2.23	-2.20	1	27	4.84	4.88	4.94	4.98
5016.17	13	uc	a^5F_5	$y^5G_5^o$	0.85		-0.518	2	65	4.83	4.86	4.91	4.95
5022.87	13	b	a^5F_3	$y^5G_3^o$	0.83		-0.38	2	74	4.83	4.87	4.92	4.96
5039.96	3	b,s	a^3F_3	$z^3D_2^o$	0.02	-1.09	-1.07	3	77	4.83	4.86	4.91	4.94
5064.65	3	b	a^3F_4	$z^3D_3^o$	0.05	-0.95	-0.94	1	84	4.88	4.91	4.99	5.01
5113.45	48	b	b^3F_3	$v^3D_2^o$	1.44		-0.727	4	27	4.77	4.79	4.86	4.88
5147.48	2	b,uc	a^3F_2	$z^3F_3^o$	0.00	-1.89	-1.95	1	38	4.73	4.78	4.83	4.88
5152.19	2	b	a^3F_3	$z^3F_4^o$	0.02	-1.90	-1.96	1	38	4.74	4.78	4.83	4.88
5173.75	2	b	a^3F_2	$z^3F_2^o$	0.00	-1.07	-1.06	1	79	4.78	4.82	4.88	4.91
5192.98	2	b	a^3F_3	$z^3F_3^o$	0.02	-0.96	-0.95	1	85	4.78	4.82	4.88	4.91
5210.39	2	b	a^3F_4	$z^3F_4^o$	0.05	-0.85	-0.82	1	88	4.84	4.88	4.94	4.97
5219.7	2	b	a^3F_3	$z^3F_2^o$	0.02	-2.26	-2.23	1	28	4.88	4.92	4.97	5.01
5295.78	31	b	a^3P_2	$x^3D_3^o$	1.07		-1.577	3	13	4.82	4.86	4.92	4.95
5490.15	45	b	b^3F_4	$x^3D_3^o$	1.46		-0.877	4	24	4.8	4.82	4.89	4.91
5662.15	78	b	$z^5D_4^o$	e^5F_5	2.32		-0.053	4	24	4.81	4.83	4.9	4.93
5866.46	30	b	a^3P_2	$y^3D_3^o$	1.07		-0.784	2	48	4.81	4.82	4.9	4.91
5922.12	27	b,uc	a^3P_0	$y^3D_1^o$	1.05		-1.410	2	21	4.84	4.87	4.93	4.96
5965.83	62	b,uc	a^3G_4	$z^3H_5^o$	1.88		-0.353	4	28	4.8	4.82	4.89	4.91
5978.54	62	a	a^3G_3	$z^3H_4^o$	1.87		-0.440	4	25	4.79	4.81	4.87	4.89
6064.63	25	b,uc	a^3P_0	$z^3S_1^o$	1.05		-1.888	3	9	4.85	4.88	4.96	5.00
6092.8	61	uc	a^3G_5	$w^3G_5^o$	1.89		-1.323	4	5	4.82	4.86	4.92	4.96
6126.22	25	a	a^3P_2	$z^3S_1^o$	1.07		-1.369	3	23	4.85	4.87	4.95	4.97
6258.71	43	a	b^3F_4	$y^3G_5^o$	1.46		-0.299	4	53	4.79	4.79	4.88	4.89
6261.1	43	b,uc	b^3F_2	$y^3G_3^o$	1.43		-0.423	4	49	4.83	4.84	4.92	4.93
6303.76	43	b,rc	b^3F_3	$y^3G_3^o$	1.44		-1.510	4	9	4.83	4.86	4.93	4.97
6312.24	43	b,rc	b^3F_4	$y^3G_4^o$	1.46		-1.496	4	9	4.81	4.84	4.9	4.94
6554.24	41	b	b^3F_3	$x^3F_3^o$	1.44		-1.162	4	11	4.83	4.86	4.91	4.94
6556.08	41	a	b^3F_4	$x^3F_4^o$	1.46		-1.018	4	11	4.81	4.83	4.89	4.91
7357.74	35	b,rc	b^3F_3	$y^3F_3^o$	1.44		-1.066	4	23	4.85	4.87	4.94	4.96
8426.51	7	b	a^5F_3	$z^5D_2^o$	0.83		-1.197	2	51	4.89	4.92	4.96	5
8435.66	7	b	a^5F_4	$z^5D_3^o$	0.84		-0.967	2	62	4.88	4.91	4.96	4.98
8682.99	24	uc	a^3P_1	$z^3D_2^o$	1.05	-1.69	-1.82	3	15	4.74	4.77	4.83	4.86

^a Line identification: a - unblended; b - blended; uc - uncertain continuum; s - saturated; rc - renormalized continuum ^b References to gf -values: (1) Blackwell et al. (1982, a); (2) Blackwell et al. (1982, b); (3) Blackwell et al. (1983); (4) Blackwell et al. (1986)

Table 2. Parameters of Ti II lines used for the spectrum synthesis and individual abundances. The lines at 4394, 4395, 4443 Å were not used in the solar abundance analysis. For some transitions Pickering et al. (2001) do not provide accuracies of *gf*-values.

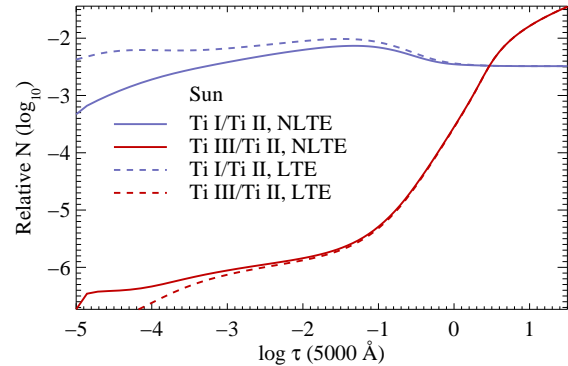
λ	Mult.	Rem. ^a	Lower level	Upper level	E_{low} [eV]	W_λ [mÅ]	$\log gf$	Unc.	Source ^b	MAFAGS-ODF		MAFAGS-OS	
										$\log \epsilon_{\text{LTE}}$	$\log \epsilon_{\text{NLTE}}$	$\log \epsilon_{\text{LTE}}$	$\log \epsilon_{\text{NLTE}}$
4394.05	12	b	$a^2P_{0.5}$	$z^4D_{1.5}^o$	1.22	77	-1.78	0.04	1				
4395.85	3	b	$b^4P_{2.5}$	$z^4D_{3.5}^o$	1.24	71	-1.93	0.04	1				
4443.8	3	b	$a^2D_{1.5}$	$z^2F_{2.5}^o$	1.08	138	-0.72	0.02	1				
4444.56	6	b	$a^2G_{3.5}$	$z^2F_{3.5}^o$	1.12	61	-2.24		1	4.97	4.97	4.99	4.99
4468.5	6	b	$a^2G_{4.5}$	$z^2F_{3.5}^o$	1.13	139	-0.6	0.02	2	4.94	4.92	4.98	4.96
4488.32	26	b,uc	$c^2D_{2.5}$	$x^2F_{3.5}^o$	3.12	50	-0.51	0.03	1	4.86	4.84	4.91	4.90
4493.52	2	b	$a^2D_{1.5}$	$z^4F_{2.5}^o$	1.08	33	-2.83	0.05	1	4.89	4.89	4.90	4.90
4563.77	11	b	$a^2P_{0.5}$	$z^2D_{1.5}^o$	1.22	129	-0.69	0.02	1	4.98	4.98	5.01	5.01
4583.41	8	b	$a^4P_{1.5}$	$z^2F_{2.5}^o$	1.17	31	-2.92		1	5.03	5.03	5.04	5.03
4636.32	7	b	$a^4P_{1.5}$	$z^4F_{2.5}^o$	1.16	20	-3.02		1	4.81	4.8	4.85	4.84
4657.2	13	b	$b^4P_{2.5}$	$z^2F_{3.5}^o$	1.24	52	-2.32	0.03	2	4.98	4.97	4.99	4.98
4708.66	10	uc	$a^2P_{1.5}$	$z^2F_{2.5}^o$	1.24	51	-2.34	0.05	1	4.96	4.95	4.97	4.96
4798.53	1	a	$a^2D_{1.5}$	$z^4G_{2.5}^o$	1.08	44	-2.68	0.08	1	4.97	4.97	5.00	5.00
5129.15	20	b	$b^2G_{4.5}$	$z^2G_{4.5}^o$	1.89	72	-1.24	0.03	1	4.96	4.93	4.99	4.96
5336.81	16	b	$b^2D_{2.5}$	$z^2F_{3.5}^o$	1.58	71	-1.63	0.03	2	5.05	5.02	5.03	5.00
5381.01	16	b	$b^2D_{1.5}$	$z^2F_{2.5}^o$	1.57	57	-1.92	0.05	1	4.95	4.94	4.95	4.94
5418.77	16	b	$b^2D_{2.5}$	$z^2F_{2.5}^o$	1.58	51	-2	0.05	1	4.90	4.89	4.90	4.89

^a Line identification: a - unblended; b - blended; uc - uncertain continuum ^b References to *gf*-values: (1) Pickering et al. (2001); (2) Bizzarri et al. (1993)

3.1 NLTE effects on atomic number densities and line formation

The qualitative analysis of level *departure coefficients*⁶ helps to understand NLTE effects in excitation and ionization balance of Ti. Departure coefficients of selected atomic energy levels of Ti I computed for MAFAGS-ODF model atmospheres⁷ with different prescriptions for elastic collisional rates are shown in Fig. 5. Fig. 4 shows relative number densities $N(\text{Ti I})/N(\text{Ti II})$ and $N(\text{Ti III})/N(\text{Ti II})$ for the solar model atmosphere computed under LTE (dashed lines) and NLTE (solid lines).

In general, most of the Ti I levels in the atmospheres of late-type stars are underpopulated relative to their LTE number densities. The driving mechanism is overionization by non-local UV radiation field with mean intensity J_ν larger than the local Planck function $B_\nu(T_e)$. However, due to the complexity of Ti atom, other NLTE mechanisms also play a role and population of each level at each atmospheric depth is determined by its collisional and radiative interaction with hundreds of other atomic states and, indirectly, even with the levels of the next ionization stage, Ti II. Thus, clear isolation of interaction processes leading to NLTE population of each atomic level is not possible and we have chosen only few Ti I and Ti II levels to illustrate the typical NLTE effects. Transitions between these levels are strong and few of them, $\lambda 4758$ Å and $\lambda 4759$ Å ($a^3H \leftrightarrow x^3H^o$), were selected for the stellar abundance analysis. Fig. 5 shows the Ti I ground state a^3F , even-parity metastable levels a^3H ($E_{\text{low}} = 2.2$ eV), odd-parity levels t^3F^o and x^3H^o ($E_{\text{low}} = 4.8$ eV and 4.85 eV, respectively). Also, few Ti II

**Figure 4.** Relative number densities $N(\text{Ti I})/N(\text{Ti II})$ and $N(\text{Ti III})/N(\text{Ti II})$ for the solar model atmosphere with parameters 5780/4.44/0 and $[\text{Ti}/\text{H}] = 4.9$, computed under LTE and NLTE.

levels, which give rise to the Ti II transitions visible in our stellar spectra, are shown.

Fig. 5a illustrates departure coefficients computed for the solar model atmosphere assuming a scaling factor $S_H = 0.05$ for the Drawin (1968) cross-sections for collisions with H I atoms and non-scaled cross-sections for transitions due to electron collisions, $S_e = 1$ (Sect. 2.3). LTE distribution functions for the Ti I are invalid already at $\log \tau_{5000} \sim +0.3$, which is where the atmosphere becomes transparent to UV continuum radiation. The super-thermal radiation field, $J_\nu > B_\nu(T_e)$, increases photoionization rates from the Ti I levels with ionization edges at relevant wavelengths, that is, at $\lambda \sim 300 - 400$ nm. Since this process is not compensated by the recombination rates, which are fixed by the local kinetic temperature T_e , the disbalance in number densities of well-populated Ti I levels with excitation energy 2 – 3 eV is transferred to the

⁶ The departure coefficients are defined as the ratio of NLTE to LTE number densities of atoms in a certain excited level i , $b_i = n_i^{\text{NLTE}}/n_i^{\text{LTE}}$ (definition according to Wijnenga & Zwaan 1972)

⁷ The choice of the ODF or OS model has no impact on the conclusions drawn in this section

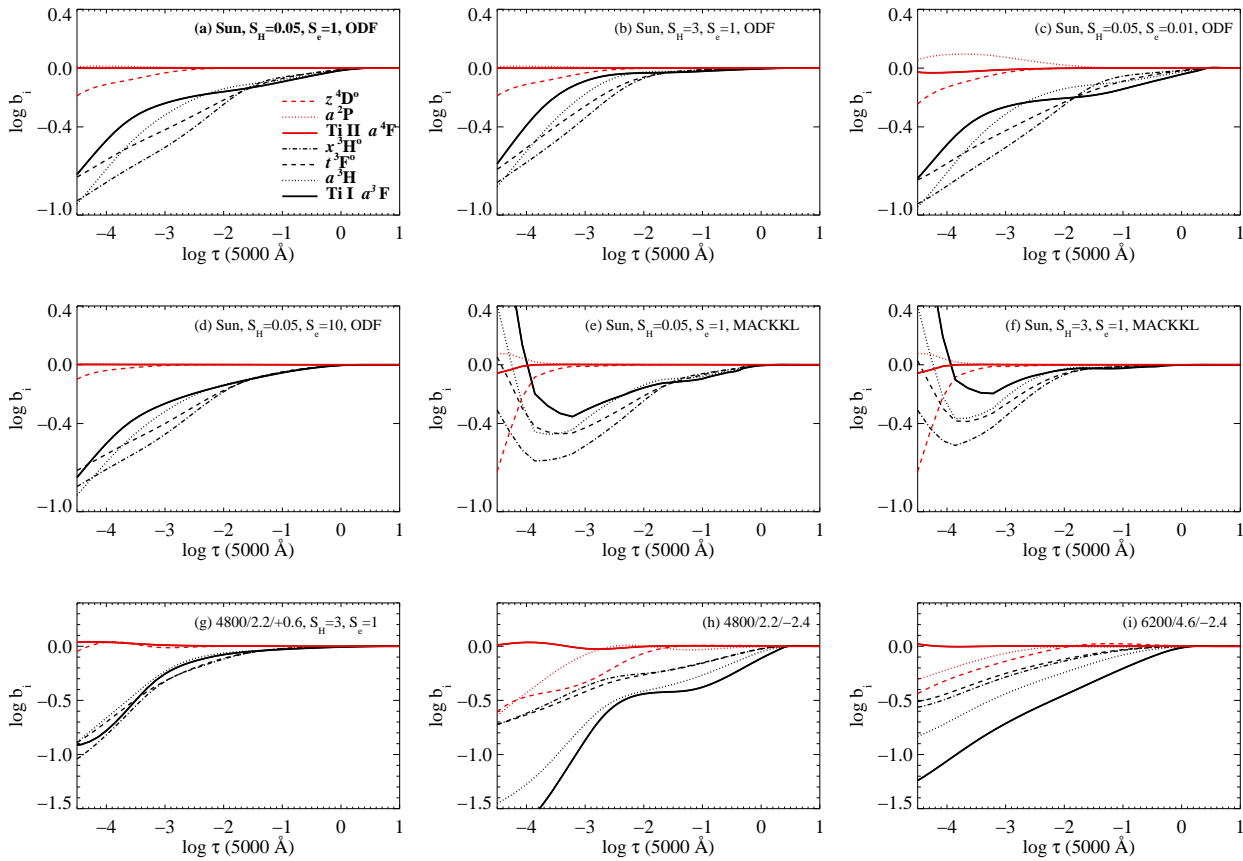


Figure 5. Departure coefficients for selected Ti I and Ti II levels computed for the MAFAGS-ODF (a)-(d) and MACKKL (e)-(f) solar model atmospheres with different prescriptions for inelastic collision rates. (g) to (i): Same as (b), but the model atmospheres are taken from the grid with stellar parameters specified in each panel. Level designations in all panels are the same as in (a). See text for details.

other levels via collisions and strong UV radiative transitions. This is an interesting case, when collisions inhibit deviations from LTE for some levels, but amplify them for the others by thermalizing the relative populations of the levels with different degree of underpopulation.

At $-1.5 \leq \log \tau_{5000} \leq 0$ in the solar case, optical depth in the strong UV transitions of Ti I is still larger than unity and photoionization cross-sections of the levels in the hydrogenic approximation are a monotonic function of frequency, $\sigma_{\text{ph-ion}} \sim 1/\nu^3$, thus underpopulation of all levels is very homogeneous. The weak Ti I lines, which are formed at these optical depths, are only affected by the change in opacity, which scales with the departure coefficient of their lower level. Since respective b_i -factors are less than unity, NLTE model lines are weaker compared to LTE and require larger Ti abundance to fit the observed spectrum. A few examples of NLTE synthetic lines of Ti I computed with the MAFAGS-ODF solar model are given in Fig. 6(a,b), where they are compared to the observed profiles. The *shapes* of line profiles computed with ODF or OS models are very similar, thus profiles computed with the latter are not shown in the Figure. The LTE profiles reproduce the NLTE profiles after adjustment of the Ti abundance and macro-turbulence.

Excitation balance in Ti I significantly deviates from thermal at $\log \tau_{5000} \leq -1.5$ for the MAFAGS solar model, where photon losses in numerous near-UV and blue transitions influence the relative populations of the levels. The majority of such transitions are

resonance (multiplet numbers 1 to 37). For example, the Ti I ground state, a^3F is radiatively connected with the t^3F^o level with the excitation energy 4.8 eV (Fig. 5 a). Although there is an ample pumping of the upper level by super-thermal J_ν at $-1 \leq \log \tau_{5000} \leq 0$, photon escape in the lines of the multiplet 30 leads to a sudden underpopulation of t^3F^o at $\log \tau_{5000} \sim -1.3$. The latter process, combined with photon losses in other resonance transitions, causes the outward flattening of the departure coefficient for the Ti I ground state a^3F , up to the depths where its b_i -factor drops again due to the dominant overionization. The same mechanism acts between the a^3H and x^3H^o levels (multiplet 114). The corresponding lines form at $\log \tau_{5000} \sim -1.2$ (Fig. 5a).

In the outermost layers, $\log \tau_{5000} \leq -3.5$, the theoretical solar model atmosphere is not adequate: it lacks chromospheres. In the MACKKL semi-empirical solar model, the temperature minimum occurs at $\log \tau_{5000} \approx -3.4$. Below this optical depth, the behaviour of departure coefficients is identical to the MAFAGS model (Fig. 5e,f). However, the outward rise of temperature leads to the overpopulation of Ti I levels, contrary to the strong underpopulation predicted by the MAFAGS models. As a result, NLTE abundance corrections change in sign and magnitude, which is particularly important for lines formed above T_{min} , such as the strong resonance Ti I lines at 3998.6 Å and 3989.76 Å. LTE abundances determined with the MACKKL and MAFAGS models also differ because the former is slightly warmer than the latter in the layers below $\log \tau_{5000} = -3$ (Fig. 1).

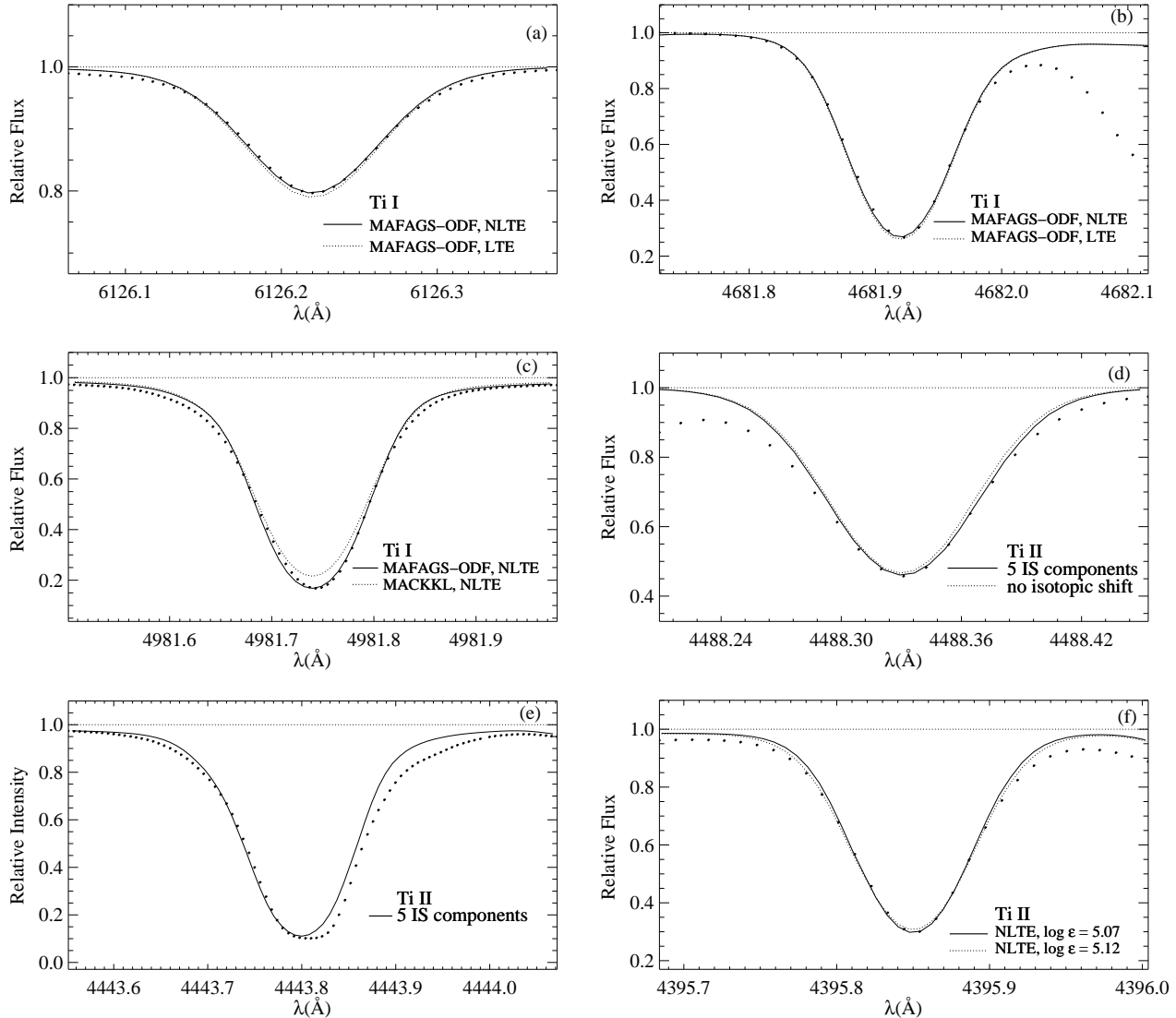


Figure 6. Synthetic (black trace) and observed (symbols) profiles of selected Ti I and Ti II lines in the solar spectrum. (d): for demonstration purposes, the theoretical profile was synthesized excluding the contribution of blends in the wings that makes the fit worse. (e): the line was not used for the solar abundance calculations due to an unknown blend. See text for details.

To illustrate the difference between the theoretical and semi-empirical models with respect to abundance determinations, we consider two Ti I lines. The line at 4981.73 Å (multiplet 44) is the strongest in our list with $W_\lambda \sim 120$ mÅ. The NLTE line profiles computed with the MAFAGS-ODF and MACKKL solar model atmospheres are compared with the observed solar flux profiles in the Fig. 6c. The NLTE abundance corrections have different signs: $\Delta_{\text{NLTE}}(\text{MAFAGS} - \text{ODF}) = +0.02$ dex and $\Delta_{\text{NLTE}}(\text{MACKKL}) = -0.05$ dex. The NLTE Ti abundances deduced from such profile fits are 4.86 dex and 4.98 dex for the MAFAGS-ODF and MACKKL models, respectively. For the weak line at 4997 Å with $W_\lambda \sim 34$ mÅ, MACKKL model also overestimates the abundance by 0.1 dex compared to the MAFAGS-ODF model, but the NLTE corrections for both model atmospheres are equal, $\Delta_{\text{NLTE}} = +0.04$ dex.

The influence of uncertainties in atomic data on the excitation and ionization balance of Ti was tested by changing the cross-sections for collision-induced transitions by hydrogen atoms and free electrons. Scaling down the cross-sections of transitions due to

e^- collisions by two orders of magnitude (Fig. 5c), $S_e = 0.01$, leads to decoupling of all levels at $\log \tau_{5000} \geq -1.5$, whereas increasing the cross-sections by a factor of ten (Fig. 5d) produces *relative* thermalization of the levels with excitation energy below 5 eV in the same range of optical depths $\log \tau_{5000}$.

Departure coefficients are very sensitive to the variation of the scaling factor to inelastic H I collisions S_H . With $S_H = 3$, the Ti I levels nearly thermalize at $-2 \leq \log \tau_{5000} \leq 0$ (Fig. 5b). It is only in the uppermost layers with low densities, $\log \tau_{5000} \leq -3$, that the influence of collisions with H I is small. We note that $S_H = 3$ produces the smallest abundance scatter between Ti I lines and simultaneously satisfies ionization balance of Ti in the solar case (Sect. 3.2). Thus, the latter value defines our reference model atom. Yet, it has to be kept in mind that calibration of S_H on the observed stellar spectrum may hide or compensate other deficiencies in the modelling, such as those related to the use of the 1D static model atmospheres with a certain prescription for convection, i.e. mixing-length theory in our case, and the fixed microturbulence parameter.

Table 3. Isotopic components of selected Ti II and Ti I transitions for the solar mixture of the isotopes. See text.

Transition	Wavelength Å	log gf_i	Isotope
Ti II			
$c^2D_{2.5} - x^2F_{3.5}^{\circ}$	4488.346	-1.607	46
	4488.337	-1.638	47
	4488.330	-0.642	48
	4488.322	-1.77	49
	4488.315	-1.78	50
$a^2G_{4.5} - z^2F_{3.5}^{\circ}$	4468.498	-1.697	46
	4468.504	-1.729	47
	4468.510	-0.732	48
	4468.515	-1.860	49
	4468.521	-1.868	50
$a^2G_{3.5} - z^2F_{3.5}^{\circ}$	4444.548	-3.337	46
	4444.554	-3.369	47
	4444.560	-2.372	48
	4444.565	-3.500	49
	4444.571	-3.507	49
Ti I			
$a^3P_2 - y^3D_3^{\circ}$	5866.440	-2.108	46
	5866.449	-2.100	47
	5866.459	-0.972	48
	5866.469	-1.977	49
	5866.480	-1.937	49
$a^3P_0 - y^3D_1^{\circ}$	5922.100	-2.734	46
	5922.109	-2.726	47
	5922.119	-1.598	48
	5922.129	-2.603	49
	5922.140	-2.563	49

Thus, our final value of S_H may not be appropriate for other NLTE studies of Ti, which are based on different model atmospheres and methods (see e.g. discussion in Asplund 2005).

We performed test NLTE calculations for several models with the following parameters: (a) $T_{\text{eff}} = 4800$, $\log g = 2.2$, $[\text{Fe}/\text{H}] = +0.6$; (b) $T_{\text{eff}} = 4800$, $\log g = 2.2$, $[\text{Fe}/\text{H}] = -2.4$; (c) $T_{\text{eff}} = 6200$, $\log g = 4.6$, $[\text{Fe}/\text{H}] = -2.4$. These parameters are representative of stars commonly used in Galactic chemical evolution studies, i.e. metal-rich K -type giants in the bulge, metal-poor giants and dwarfs in the halo. Departure coefficients for the three models computed with $S_H = 3$ and $S_e = 3$ are shown in Fig. 5. A rather counter-intuitive result is that the Ti I and Ti II level populations show departures from LTE even for the cool giant with super-solar metallicity (Fig. 5g). Even though UV radiation field is weakened due to low photospheric temperatures and excessive line blanketing, collisions at $\log g \approx 2$ are too weak to ensure LTE conditions. Since the stellar flux maximum is shifted to longer wavelengths, ionization from the Ti I levels with higher excitation potential, e.g. a^3H , becomes more important compared to the solar case. Qualitatively, our results for cool stars of solar metallicity are very similar to Hauschildt et al. (1999, their Fig. 4).

NLTE effects are particularly large for the metal-poor models with low gravity (Fig. 5h). NLTE number densities of the majority of Ti I levels are reduced by a factor of 2 already at $\log \tau_{5000} \sim -0.5$. The undulations of the b_i -curves with $\log \tau_{5000}$ are due to strong ra-

diative interaction between levels, i.e. non-balanced excitations at the depths where photons escape in the wings of strong Ti I lines and spontaneous de-excitations at the core formation depths. In contrast, very homogeneous distribution of b_i -factors with optical depth is characteristic of warm high-gravity models (Fig. 5i). This is an expected result, because collisions provide close coupling of the levels and even the Ti I ground state with the largest occupation number is subject to overionization caused by strong non-local UV radiation field near its ionization threshold.

Deviations from LTE in Ti II are small for the combinations of stellar parameters investigated in this work. Departure coefficients of low and intermediate-excitation Ti II levels deviate from unity in the upper atmospheric layers, at $\log \tau_{5000} \leq -2$. Most of the Ti II lines form below this depth, where b_i -factors are slightly larger than unity, and the corresponding effect on abundances is never larger than -0.05 dex.

3.2 The Sun

3.2.1 Spectrum synthesis

The solar abundance of Ti was determined by visually fitting synthetic spectral lines computed with LTE or NLTE number densities to the Solar Flux Atlas of Kurucz et al. (1984). We used both MAFAGS-ODF and MAFAGS-OS model atmospheres. The standard line broadening mechanisms were taken into account: solar rotation with $V_{\text{rot},\odot} = 1.8 \text{ km s}^{-1}$, microturbulence velocity $\xi_t = 0.9 \text{ km s}^{-1}$, and a radial-tangential macroturbulence velocity $\xi_{\text{RT}} = 2.5 \dots 4 \text{ km s}^{-1}$. Line broadening caused by elastic collisions with H I atoms was computed using the velocity parameters and temperature exponents from Anstee & O'Mara (1995). In Tables 1 and 2, this parameter is given in terms of the van der Waals damping constant $\log C_6$ for each transition.

3.2.2 Oscillator strengths

Oscillator strengths for the Ti II transitions were adopted from Pickering, Thorne & Perez (2001), who combined their branching ratios obtained by the methods of Fourier transform spectrometry with the radiative lifetimes measured by means of time-resolved laser-induced fluorescence by Bizzarri et al. (1993). The accuracy of the latter is about 5%. We also used the $\log gf$ values of Bizzarri et al. (1993). The oscillator strengths from both sources agree well with each other for $\log gf > -1.5$ (Pickering et al. 2001, their Fig. 3), but significant discrepancies, up to 0.3 dex, are present for the weaker transitions. The uncertainties of gf -values from both references are typically less than 0.05 dex, but for some transitions experimental error was as large as 0.2 dex.

For the Ti I transitions, we relied on the oscillator strengths of Blackwell-Whitehead et al. (2006), who applied the same experimental techniques as Pickering et al. (2001). As a test case, we also used the gf -values of Blackwell et al. (1982a, 1982b, 1983, 1986), which we corrected by $+0.056$ as recommended by Grevesse, Blackwell & Petford (1989), who renormalized the relative oscillator strengths measured with the Oxford furnace to more accurate lifetimes of Rudolph & Helbig (1982). The estimated errors of the absolute f -values are less than 5%.

All parameters of the selected lines, including different sets of oscillator strengths, are given in Tables 1 and 2. Given the above-mentioned discrepancies between oscillator strengths from different experimental sources, we decided to compute the average Ti abundance for each set of gf -values.

Table 4. Solar abundance of Ti computed with different NLTE model atoms and model atmospheres. The brackets specify a combination (S_H, S_e) used for each model atom. See texts.

Ion	N	gf^a	MAFAGS-ODF				MAFAGS-OS				
			LTE	(3, 1)	LTE	(3, 0.01)	(3, 1)	(3, 10)	(0.05, 0.01)	(0.05, 1)	(0.05, 10)
Ti I	12	1	4.80 ± 0.05	4.84 ± 0.05	4.90 ± 0.05	5.01 ± 0.08	4.94 ± 0.05	4.95 ± 0.05	5.11 ± 0.06	5.02 ± 0.05	5.01 ± 0.05
	52	2	4.81 ± 0.03	4.84 ± 0.03	4.91 ± 0.04	4.95 ± 0.06	4.93 ± 0.04	4.93 ± 0.05	5.09 ± 0.09	5.00 ± 0.05	5.00 ± 0.04
Ti II	10	3	4.94 ± 0.06	4.93 ± 0.07	4.96 ± 0.06		4.95 ± 0.06				
	11	4	4.98 ± 0.04	4.97 ± 0.04	4.99 ± 0.04		4.98 ± 0.04				

^a References: (1) Blackwell-Whitehead et al. (2006); (2) Blackwell et al. (1982a, 1982b, 1983, 1986), scaled by +0.056 dex following Grevesse et al. (1989); (3) Pickering et al. (2001); (4) Bizzarri et al. (1993)

3.2.3 Abundance of Ti in the solar photosphere

The mean Ti abundances obtained under LTE and NLTE with different model atmospheres, model atoms, and sets of oscillator strengths are given in Table 4. The individual abundances for each spectral line are listed in Tables 1 and 2. NLTE abundances given in these tables were derived assuming efficient inelastic H - Ti collisions in statistical equilibrium calculations, $S_H = 3$. The choice of the scaling factor will be described below.

In Table 4, it can be seen that the LTE abundances determined from the Ti I lines are systematically lower than the NLTE abundances, with the difference of 0.05 – 0.1 dex, which depends on the treatment of inelastic collisions in statistical equilibrium calculations. Also, the MAFAGS-ODF model atmosphere underestimates the solar Ti abundance by ~ 0.1 dex compared to the MAFAGS-OS model. This is due to differences in the temperature and pressure structure of the models (Fig. 1). The NLTE values determined from the Ti I lines using the Blackwell-Whitehead et al. (2006) and Blackwell et al. (1982a, 1982b, 1983, 1986) gf values agree well with each other. Mean LTE abundances deduced with either of the gf sets are also consistent. Blackwell-Whitehead et al. (2006) noted that the gf -values for several near-IR transitions of Ti I measured by Blackwell et al. (1983) are inaccurate due to non-equilibrium effects in the Oxford furnace, and should be modified by $\sim 50\%$. Our results do not allow to confirm or refute this statement, since in both cases the individual abundances for the near-IR transition $a^3P_1 - z^3D_2^o$ (8683 Å) differ by more than 1σ from the mean value computed for a corresponding $\log gf$ set (Table 1).

NLTE abundances for each Ti I line derived with the MAFAGS-OS model atmosphere and different atomic models (described in Sect. 2.3) are shown in Fig. 7 as a function of line equivalent width, oscillator strength, and excitation potential of the lower level of the transition. The combination of the scaling factors S_H and S_e used for each model atom is indicated in the first panel of each row. The case of (0.05, 10) is omitted because the results are almost identical to the case (0.05, 1) (Fig. 7e). LTE results are also presented. Filled symbols denote the values computed with the $\log gf$ set from Blackwell et al. (1982a, 1982b, 1983, 1986), and open symbols correspond to the individual abundances derived with the data from Blackwell-Whitehead et al. (2006). There are 12 lines in common between the two experimental studies. Dashed lines show the average NLTE abundance determined for each atomic model with the gf -values of Blackwell et al., (4). We do not present analogous plots for the Ti II-based abundances because NLTE effects on Ti II in the solar case are negligibly small, which is evident from Table 4.

Inspection of NLTE $\log \epsilon_{Ti}$ values in Fig. 7 shows that NLTE abundances are very sensitive to the atomic data used in statistical

equilibrium calculations. For some combinations of S_H and S_e , e.g. (3, 0.01)(Fig. 7a) and (0.05, 0.01) (Fig. 7d) the scatter between the Ti I lines is very large. The individual abundances differ by a factor of two, although there are no physically significant trends with the equivalent width. In addition, abundance seems to be correlated with the oscillator strength and excitation potential of the lower level, if only the gf -values of Blackwell et al. (1982a, 1982b, 1983, 1986) are considered. The gf - $\log \epsilon$ and E_{low} - $\log \epsilon$ slopes are larger for the cases (a) and (d) that clearly gives rise to the large spread of abundance with W_λ . On the one side, this is an irrefutable argument against small scaling factors to e^- collision rates, e.g. $S_e = 0.01$. One could also argue that small S_H values are inappropriate, because they lead to uncomfortably large solar Ti abundances (Table 4), ≥ 5.00 , which are not consistent with the meteoritic value⁸. However, the latter depends on the solar abundance of the reference element Si, which may be subject to usual problems of spectroscopic methods as well (Asplund 2000; Shi et al. 2008). A second possibility is that the Ti model atom is incomplete in terms of number of levels and transitions. Mashonkina et al. (2010) have recently demonstrated that it is important to include highly-excited *predicted* levels and transitions between them in statistical equilibrium calculations for Fe. Although these data also exist for Ti, the number of predicted levels and transitions exceeds 14 000 and few millions, respectively. Even more levels and radiative transitions are predicted for Fe I: $\sim 37\,500$, respectively, ~ 6 millions. Such atomic models are not tractable even with 1D NLTE codes and require efficient algorithms to reduce them by combining the levels and lines. We are currently working on this.

It has to be kept in mind that photoionization cross-sections are also not appropriate for Ti. However, in the absence of quantum-mechanical calculations, it is impossible to predict whether the hydrogenic approximation over- or underestimates the cross-sections. We conclude this in analogy to the similar atom Cr I, for which the calculated photoionization cross-sections of Nahar (2009) differ from the hydrogenic approximation by orders of magnitude, being significantly larger for some levels and smaller for others. In principle, the same is true for the electron and H I collision rates. Comparison of R-matrix calculations for e^- collisions for Ca II (Meléndez, Bautista & Badnell 2007) with the formula of van Regemorter (1962) also reveals order of magnitude differences. What concerns inelastic H I collision, compared to the Drawin's formulas, *ab initio* quantum-mechanical calculations predict significantly lower collision rates for certain transitions of simple alkali atoms (Belyaev & Barklem 2003; Barklem et al. 2010), and they

⁸ $\log \epsilon = 4.91 \pm 0.03$ dex (Asplund et al. 2009)

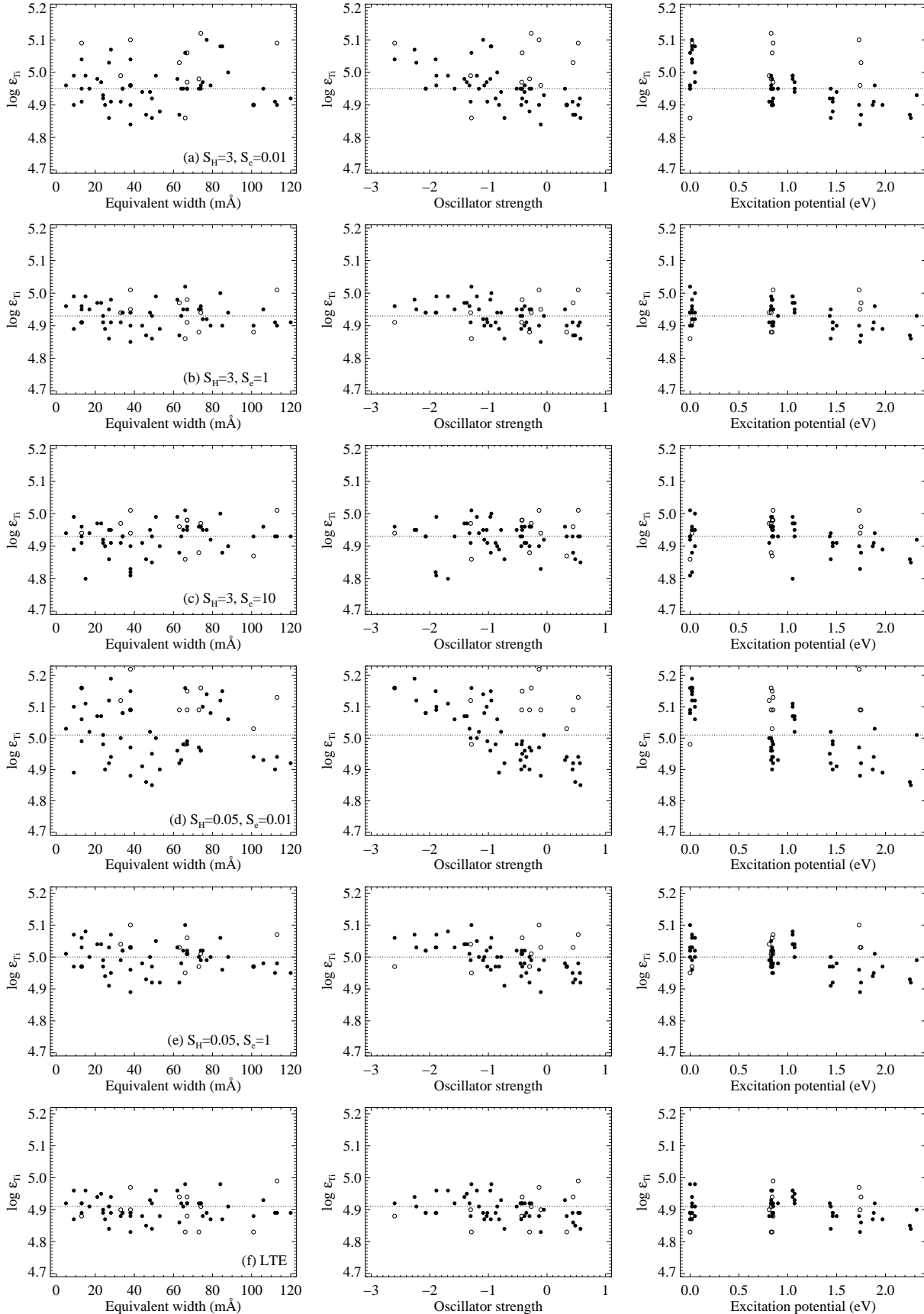


Figure 7. NLTE Ti abundances computed with the MAFAGS-OS solar model and different model atoms. Filled symbols denote the values computed with the $\log gf$ set from Blackwell et al. (1982a, 1982b, 1983, 1986), and open symbols correspond to the abundances derived with the data from Blackwell-Whitehead et al. (2006).

show that, in addition to excitation, other effects like ion-pair formation become important.

There are also other explanations for the apparent trends of individual abundances with the parameters of Ti I lines and/or large scatter, which are not related to the deficiencies of NLTE modelling. First, one can question the reliability of statistics based on small number of lines, i.e. there are just few lines in our list with small $\log gf$'s. Also, the range of low-level excitation potentials is limited to 0 – 2.5 eV. Second, the uncertainties of gf -values from Blackwell et al. (1982a, 1982b, 1983, 1986) might be underestimated. It is interesting that the same regularity, i.e. variation of abundance with multiplet, was also found in the LTE analysis of solar Ti I lines by Blackwell et al. (1987, their Fig. 4), and it is present for the individual Ti abundances based on the LTE assumption (Fig. 7f) and/or the MAFAGS-ODF model atmosphere. In addition to uncertainties in the gf values measured with the Oxford furnace, Blackwell et al. (1987) also suggested that some Ti I lines are affected by photospheric temperature and velocity fluctuations, which are very pronounced in 3D hydrodynamical solar model atmospheres (Asplund 2005). Although this is most likely the case for low-excitation temperature-sensitive lines, we do not see any trend of abundance with line strength (Fig. 7a). The latter probably indicates that a single depth-independent microturbulence is not a bad approximation. Otherwise, the medium-strong lines ($W_\lambda \approx 60 \dots 100$) being very sensitive to ξ_t would show systematically higher (or lower) abundances.

The abundances derived from the NLTE and LTE profile fitting of the Ti II lines are given in Table 4. Although the standard deviations of the mean abundances, especially for the gf -values of Pickering et al. (2001), are quite large, there is no trend of individual line abundances with E_{low} , W_λ and $\log gf$ (not shown). As expected from the results of Sect. 3.1, LTE abundances are slightly larger than that computed under NLTE. The effect of the isotopic shift on the abundance determinations is not negligible. For example, a single component used to fit the observed Ti II line at 4488 Å, overestimates the abundance by 0.06 dex compared to the result obtained with 5 isotopic components (Fig. 6d). To demonstrate that the profile composed of several components is also slightly asymmetric, the Ti II line was plotted excluding the contribution of blends in the wings.

Some Ti II lines require very large abundances, $\log \varepsilon \geq 5.05$ dex, to fit their profiles in the solar flux spectrum. Few of them also demonstrate broad asymmetric cores in the solar disk-center intensity spectrum, which can not be reproduced even taking isotopic structure into account. One of these lines, 4443 Å, with an isotopic shift of ~ 380 MHz (Nouri et al. 2010) is shown in Fig. 6e. Very specific profile shapes are probably not due to convective motions (Asplund et al. 2000). Thus, we neglect such lines in the solar analysis assuming that they contain unresolved blends in the inner cores⁹. The synthetic profiles of other discrepant lines systematically underestimate depths of both wings, e.g. 4395 Å (Fig.

⁹ The presence of blends can be revealed either by searching for asymmetries in the observed line profiles or by inspecting theoretical line lists. One problem is that often weak blends overlap with the core of a stronger line under investigation that leaves the profile of the latter fully symmetric. Another problem is that theoretical line lists are compiled from transitions observed in laboratory conditions, which do not correspond to astrophysical conditions. A comparison of observed and *synthetic* spectra proves that many observed lines still lack identification, which may well contribute to the well-known “missing UV opacity” problem in the UV. It is natural to expect missing opacity in other spectral regions as well.

6f). Thus, the abundance estimate inferred from such profile fits is rather subjective and depends, among other parameters, on the adopted value for the macro-turbulence, which otherwise would not affect determination of the abundance being an external line broadening mechanism. We refrain from using these lines in the solar analysis, also because they are very sensitive to ξ_t .

In Table 4, it can be seen that MAFAGS-OS model and NLTE line formation with $S_H = 3$ achieve good ionization equilibrium of Ti I/Ti II for the Sun. For the given S_H , the mean abundances determined with $S_e = 0.01, 1, 10$ are also consistent with the Ti II-based abundances within their respective uncertainties, however $S_e = 1$ provides the smallest abundance spread for the solar case. With respect to the Ti I lines, almost equal mean abundances were obtained for the gf -values from Blackwell-Whitehead et al. (2006) and Blackwell et al. (1982a, 1982b, 1983, 1986), the latter data scaled by +0.056 dex. However, our results for the Ti II lines favour the gf -values of Pickering et al. (2001), which lead to a better agreement between the two ionization states. The MAFAGS-OS NLTE abundances, whether based on Ti I or Ti II lines, also agree well with the Ti abundance in C I meteorites, $\log \varepsilon = 4.91 \pm 0.03$ dex (Asplund et al. 2009).

3.3 Ti ionization equilibrium for the metal-poor stars

3.3.1 Observations and stellar parameters

To test ionization equilibrium of Ti in the atmospheres with reduced metal content, we have chosen four stars from the sample of Bergemann & Gehren (2008). The reader is referred to this paper for a detailed description of observations. The spectra of HD 84937, HD 140283, and HD 122563 were taken from the UVESPOP survey (Bagnulo et al. 2003). The spectra of HD 102200 were taken by T. Gehren and colleagues on the ESO UVES echelle spectrograph at the VLT UT2 in Paranal, Chile. The UVES spectra have a slit-determined resolution of $\lambda/\Delta\lambda \sim 50\,000$ and a signal-to-noise ratio better than $S/N \sim 300$ near 5000 Å.

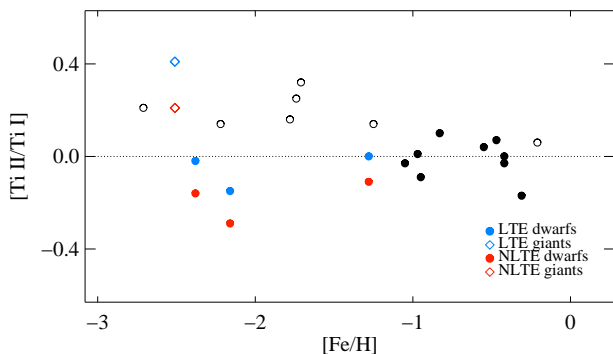
Stellar parameters were adopted from Gehren et al. (2004, 2006) for HD 84937, HD 140283, and HD 102200, and from Mashonkina et al. (2008) for HD 122563. These studies used the same observed spectra, model atmospheres (MAFAGS-ODF), and the codes as adopted in this work that secures consistency of our abundance analysis. The effective temperatures T_{eff} were determined from Balmer line profile fits, and gravities $\log g$ were based on *Hipparcos* parallaxes from the ESA (1997) catalogue. The spectroscopic temperatures are consistent with T_{eff} 's determined by Casagrande et al. (2010) using the Infrared Flux method. Casagrande et al. (2010) derived $T_{\text{eff}} = 6155$ K for HD 102200, $T_{\text{eff}} = 5777$ K for HD 140283, and $T_{\text{eff}} = 6408$ K for HD 84937. The iron abundance and microturbulence velocities were derived from LTE fitting of Fe II lines, which do not suffer from NLTE effects for the range of stellar parameters investigated here (Mashonkina et al. 2010).

MAFAGS-OS model atmospheres are available only for HD 84937 and HD 122563 (L. Mashonkina, private communication). The gravities adopted for the MAFAGS-OS models are on average ~ 0.1 dex larger than that used to compute the MAFAGS-ODF model atmospheres. The reason is that new reduction of *Hipparcos* data (van Leeuwen 2007) revealed some errors in the earlier version of the catalogue (ESA 1997). However, for our stars the parallax differences between both catalogue versions are within the parallax error itself, which propagates into 0.1 dex error in $\log g$.

Stellar parameters are given in Table 5. The estimated errors

Table 5. Stellar parameters for the selected sample. See text.

Object	MAFAGS-ODF			MAFAGS-OS			ξ_t km/s	[α /Fe]
	T_{eff}	$\log g$	[Fe/H]	T_{eff}	$\log g$	[Fe/H]		
HD 84937	6350	4.00	-2.16	6350	4.09	-2.15	1.8	0.4
HD 102200	6120	4.17	-1.28				1.4	0.4
HD 122563	4600	1.50	-2.51	4600	1.60	-2.50	1.9	0.2
HD 140283	5773	3.66	-2.38				1.5	0.4


Figure 8. NLTE (red symbols) and LTE (blue symbols) abundances of Ti in the metal-poor stars. For comparison, the LTE abundance ratios of Gratton & Sneden (1991) are shown with open and filled black symbols, respectively.

are 100 K for T_{eff} , 0.1 dex for $\log g$, 0.1 dex for [Fe/H], and 0.2 km/s for ξ_t .

3.3.2 Ti abundances in the metal-poor stars

The analysis of the metal-poor stars is differential with respect to the Sun. An individual abundance derived for each line in a stellar spectrum is related to the solar abundance from that line computed with the same parameters and assumptions in the spectrum synthesis, including model atmosphere type (OS or ODF). The Ti abundance in a star relative to the Sun is given by:

$$[\text{Ti}/\text{H}] = \log(gf\varepsilon) - \log(gf\varepsilon)_\odot$$

We also used several Ti II lines (4394.05, 4395.85, 4443.8 Å), which have been excluded from the solar abundance analysis because of profile distortions, which are likely caused by blends (Fig. 6e) and sensitivity of profile wings to microturbulence (Fig. 6f). However, in spectra of very metal-poor stars the lines are much weaker and appear to be symmetric showing no evidence for blends. Here, we discuss the stellar Ti abundances normalized to the Fe abundance of a star, [Ti/Fe]; this parameter is relevant to Galactic chemical evolution studies.

The Ti abundances determined for four metal-poor stars are given in Table 6. Fig. 8 displays the difference between [Ti/Fe] ratios computed from the lines of two ionization stages, [Ti_{II}/Ti_I] = [Ti_{II}/Fe] - [Ti_I/Fe], as a function of stellar metallicity. NLTE and LTE ratios for the metal-poor stars are shown with red and blue symbols, respectively. The figure also includes LTE Ti

abundances in metal-poor giants and dwarfs from the study of Gratton & Sneden (1991). They define stars with $\log g < 3$ giants.

Our LTE abundances based on Ti I and Ti II lines agree within their respective uncertainties for three stars, except for the very metal-poor giant HD 122563. In contrast, ionization equilibrium is not satisfied under NLTE with $S_{\text{H}} = 3$ and $S_{\text{e}} = 1$. Except for the metal-poor giant, the Ti I lines give systematically higher abundances than Ti II lines. Assuming any other combination of collision scaling factors makes the discrepancy for the three stars worse because NLTE effects on Ti I increase more for the metal-poor stars than for the Sun. Variation of S_{e} has almost no effect on the Ti abundances, whereas decreasing the efficiency of hydrogen collisions by few orders of magnitude, $S_{\text{H}} = 0.05$, leads to extreme overionization from the lowest Ti I states. This is expected because concentration of free electrons in metal-poor atmospheres is very low and thermalization of levels can only occur due to H I - atom collisions. As a result, the NLTE abundances determined with $S_{\text{H}} = 0.05$ are on average 0.2 dex larger than those computed with $S_{\text{H}} = 3$, and the difference between the latter and the LTE-based abundances is of the same order.

For HD 84937, our Ti II-based LTE abundance is 0.15 dex lower than the LTE abundance determined from the Ti I lines. This discrepancy has no relation to NLTE effects, because there is no physical mechanism to produce overpopulation of low-lying Ti I levels at expense of Ti II in the atmospheres, where Ti I is the minor ionization stage. For HD 122563, we encounter a different problem: the NLTE abundance determined from the Ti I lines is 0.2 dex lower than that from the Ti II, although the discrepancy is twice as small compared to LTE.

Thus, it appears that our reference NLTE model overestimates NLTE effects on Ti in high-gravity atmospheres, corresponding to dwarfs, however it underestimates overionization in the atmospheres of giants. For metal-poor dwarfs and subgiants, nearly thermalized occupation numbers for Ti I levels are necessary to satisfy ionization balance. As seen in Fig. 8, the results of Gratton & Sneden (1991) support this conclusion. In their LTE analysis of metal-poor stars, the mean difference between ionized and neutral species is $+0.07 \pm 0.03$ dex for dwarfs and $+0.2 \pm 0.03$ dex for giants. As noted above (Sect. 1), similar offsets for metal-poor giants were also reported in the LTE studies by Brown et al. (1983), Johnson (2002), and Tafelmeyer et al. (2010).

3.3.3 Discussion

The analysis of four metal-poor stars showed that the LTE approximation in Ti line formation calculations is not adequate for evolved stars. However our NLTE models with available atomic data for Ti do not perform better if both evolved and unevolved stars are considered. In fact, there are few reasons why the problem can still be attributed to deficiencies of the NLTE model.

All lines detected in the stellar spectra originate from the metastable levels $a^5F_{3,4,5}$ with the excitation energy ~ 0.8 eV. These levels, among many other low-lying states, dominate ionization balance in Ti I. Thus, inadequate results may reflect erroneous photoionization cross-sections, which are computed in the hydrogenic approximation. We have performed a test decreasing the cross-sections for several low-excitation Ti I states, including a^5F , by three orders of magnitude. Although the individual line abundances decrease by ~ 0.03 dex, this is by far insufficient to bring two ionization stages in agreement. We conclude that it is a cumulative effect of non-hydrogenic photoionization in Ti I, rather than cross-sections for individual atomic levels, that may lead to a

quantitatively different distribution of atomic level populations. In the absence of quantum-mechanical calculations, it is impossible to predict whether the hydrogenic approximation over- or underestimates the cross-sections for each Ti I level. Therefore, we can not explore this possibility further.

If the problem is in NLTE, then it is likely that NLTE modelling of a similar atom, Fe, suffers from similar deficiencies as Ti. For example, accurate cross-sections for transitions caused by inelastic H I and e^- collisions are missing for both atoms, and calibration of collision efficiency on observed spectra is necessary. In this case, one would expect the problem to be reduced or even eliminated if one compares the abundances determined from lines of equal ionization stages, i.e. Ti I and Fe I. The NLTE abundances based on Fe I lines and MAFAGS-OS model atmospheres¹⁰ are available only for HD 84937 and HD 122563, $[Fe_I/H] = -2.00 \pm 0.07$, respectively, $[Fe_I/H] = -2.61 \pm 0.09$ (L. Mashonkina, private communication). The former value is 0.15 dex higher than our standard Fe II-based value for the metal-poor subdwarf, $[Fe/H] = -2.15$. For the metal-poor giant, the NLTE Fe abundance determined from Fe I lines is 0.11 dex lower than the reference Fe II-based value $[Fe/H] = -2.50$. It is interesting that Fe abundances derived from the NLTE analysis of Fe I lines are slightly discrepant with that derived from Fe II lines, and the sign of discrepancy is the same as for Ti both for the dwarf and giant stars. As a result, the $[Ti/Fe]$ ratios for the two metal-poor stars determined from the NLTE analysis of Ti I and Fe I lines agree much better with that obtained from Ti II and Fe II lines. For a subdwarf HD 84937, we obtain $[Ti_I/Fe_I] = +0.44 \pm 0.02$, which is consistent with $[Ti_{II}/Fe_{II}] = +0.35 \pm 0.07$ within the respective uncertainties of both values. For a giant HD 122563, $[Ti_I/Fe_I] = +0.23 \pm 0.15$ and $[Ti_{II}/Fe_{II}] = +0.22 \pm 0.02$. Although the standard deviations of abundances are still large, the NLTE approach in this case has the advantage that it minimizes offsets between two ionization stages of Ti for both evolved and main sequence stars.

There is also some similarity between our results, i.e. an apparent need for the high degree of thermalization of Ti I levels in the atmospheres of dwarfs, and that of Korn, Shi & Gehren (2003), who investigated kinetic equilibrium of Fe in metal-poor stars with the same methods, model atmospheres, and codes, as we do. They find that a very large scaling factor to Drawin's H I collision rates, $S_H = 3$, in addition to the enforced thermalization of the upper Fe I levels (Gehren et al. 2001), is necessary to fulfill ionization equilibrium of Fe in their sample of dwarfs and subgiants with $[Fe/H] < -1$. Their results also indicate that NLTE effects on Fe II are negligible, which is supported by the results of Mashonkina et al. (2010) for Fe and is also true for Ti II (Table 6).

We conclude that the ratios $[Ti/Fe]$ in a stellar atmosphere computed exclusively using Ti II and Fe II lines should be robust, at least in the framework of 1D modelling, and should be used for Galactic chemical evolution studies, whenever possible. It is strongly recommended to avoid Ti I lines, as well as to take average of two ionization stages, in abundance analyses and in determination of surface gravity for evolved stars. Otherwise, systematic offsets between giants and dwarfs are unavoidable and will produce spurious abundance trends with metallicity.

4 SUMMARY

Statistical equilibrium of Ti was computed for a restricted range of stellar parameters, focussing on late-type stars. The Ti model atom was constructed with available experimental atomic data for levels and radiative transitions. Photoionization was assumed hydrogenic, except for the few Ti I levels, for which we adopted experimental cross-sections from Yang et al. (2009). Inelastic H I collision rates were computed following the classical Drawin (1968) formalism in the version of Steenbock & Holweger (1984). The Drawin's cross-sections were increased by a factor of three, $S_H = 3$, because this value produced the smallest abundance scatter and satisfied ionization equilibrium of Ti I/Ti II for the Sun.

NLTE effects on Ti I level populations and lines are significant for any combination of T_{eff} , $\log g$, and $[Fe/H]$. The dominant effect is overionization that makes NLTE particularly important at low metallicity. In the solar case, LTE approach underestimates the abundances by 0.05 – 0.1 dex. The solar Ti abundances derived from NLTE profile fitting of Ti I and Ti II lines with MAFAGS-OS theoretical model atmosphere are $\log \epsilon = 4.94 \pm 0.05$ dex ($\log gf$'s from Blackwell-Whitehead et al. 2006) and $\log \epsilon = 4.95 \pm 0.06$ dex ($\log gf$'s from Pickering et al. 2001). Both values agree well with the Ti abundance in C I meteorites, $\log \epsilon = 4.91 \pm 0.03$ dex (Asplund et al. 2009). The results obtained with gf -values for Ti I transitions measured with Oxford furnace (Blackwell et al. 1986, and earlier references) are identical, $\log \epsilon = 4.93 \pm 0.04$ dex. The gf -values for Ti II transitions from Bizzarri et al. (1993) lead to ~ 0.04 dex larger solar Ti abundances. MAFAGS-ODF models and/or LTE approach do not perform as good as MAFAGS-OS and NLTE with calibrated collision efficiency.

Ti abundances were computed for four metal-poor stars: HD 102200, HD 84937, HD 140283, HD 122563. LTE approach leads to an agreement between Ti I and Ti II-based abundances for unevolved stars, however it produces large discrepancy for giants. The same problem was also reported in other LTE studies of Ti abundances in metal-poor stars. Under NLTE, the discrepancy between the two ionization stages is significantly reduced for giants. However, now the Ti I lines give higher abundances than the Ti II lines for dwarfs and subgiants. This failure should by no means be seen as invalidity of the NLTE approach, but rather as a manifestation of inaccurate or missing atomic data. It is probably important to include highly-excited predicted levels and transitions between them in the model atom. In addition, accurate photoionization cross-sections and cross-sections for inelastic collisions with H I atoms are urgently needed.

One of 'temporary' solutions might be to relate NLTE abundances determined from lines of equal ionization stages, i.e. Ti I and Fe I. In our preliminary tests, the $[Ti/Fe]$ ratios for the metal-poor dwarf HD 84937 and giant HD 122563 determined from the NLTE analysis of Ti I and Fe I lines agree with those obtained from Ti II and Fe II lines. However, the standard deviations of abundances are not small. Also, one has to keep in mind the remaining discrepancy between Fe I and Fe II lines.

At present, we strongly recommend to disregard Ti I lines in abundance analyses of giants, as well as in calibration of their surface gravities. Since the NLTE effects on Ti II and Fe II are small for the range of stellar parameters investigated in this work, the ratios $[Ti/Fe]$ computed exclusively using Ti II and Fe II lines should be robust and should be used for Galactic chemical evolution studies.

¹⁰ Gehren et al. (2004, 2006) do not provide estimates of NLTE Fe abundances based on Fe I lines and MAFAGS-ODF model atmospheres for the stars in our sample.

Table 6. Ti abundances for the selected sample.

Object	[Fe/H]	[Mg/Fe]	N_{TiI}	[TiI/Fe] ODF		N_{TiII}	[TiII/Fe] ODF		[TiI/Fe] OS		[TiII/Fe] OS	
				LTE	NLTE		LTE	NLTE	LTE	NLTE	LTE	NLTE
HD 84937	-2.16	0.32	7	0.49 ± 0.02	0.63 ± 0.02	6	0.34 ± 0.08	0.34 ± 0.09	0.46 ± 0.02	0.59 ± 0.02	0.35 ± 0.06	0.35 ± 0.07
HD 102200	-1.28	0.34	16	0.28 ± 0.03	0.39 ± 0.05	11	0.28 ± 0.05	0.28 ± 0.04				
HD 140283	-2.38	0.43	5	0.19 ± 0.03	0.34 ± 0.02	6	0.17 ± 0.07	0.18 ± 0.08				
HD 122563	-2.51	0.45	5	-0.12 ± 0.07	0.13 ± 0.11	3	0.29 ± 0.03	0.34 ± 0.03	-0.19 ± 0.6	0.12 ± 0.15	0.21 ± 0.02	0.22 ± 0.02

ACKNOWLEDGMENTS

This work is based on observations collected at the European Southern Observatory, Chile, 67.D-0086A, and the Calar Alto Observatory, Spain. We thank Dr. Lyudmila Mashonkina for the MAFAGS-OS model atmospheres for selected stars. We thank Dr. Aldo Serenelli and Prof. Martin Asplund for revision of the manuscript and interesting suggestions. The detailed review by an anonymous referee helped to significantly improve the paper.

REFERENCES

- Abt A., 1952, *AJ*, 57, 158
- Allen C. W., 1973, *Astrophysical quantities*. London: University of London, Athlone Press, 1973, 3rd ed.
- Anstee S. D., O'Mara B. J., 1995, *MNRAS*, 276, 859
- Asplund M., 2000, *A&A*, 359, 755
- Asplund M., 2005, *ARAA*, 43, 481
- Asplund M., Grevesse N., Sauval A. J., Scott P., 2009, *ARAA*, 47, 481
- Asplund M., Nordlund Å., Trampedach R., Allende Prieto C., Stein R. F., 2000, *A&A*, 359, 729
- Bagnulo S., Jehin E., Ledoux C., Cabanac R., Melo C., Gilmozzi R., The ESO Paranal Science Operations Team 2003, *The Messenger*, 114, 10
- Barklem P. S., Belyaev A. K., Dickinson A. S., Gad ea F. X., 2010, *A&A*, 519, A20+
- Belyaev A. K., Barklem P. S., 2003, *Phys. Rev. A*, 68
- Berengut J. C., Flambaum V. V., Kozlov M. G., 2008, *Journal of Physics B Atomic Molecular Physics*, 41, 235702
- Bergemann M., Cescutti G., 2010, *ArXiv e-prints*
- Bergemann M., Gehren T., 2008, *A&A*, 492, 823
- Bergemann M., Pickering J. C., Gehren T., 2010, *MNRAS*, 401, 1334
- Bernkopf J., 1998, *A&A*, 332, 127
- Bizzarri A., Huber M. C. E., Noels A., Grevesse N., Bergeson S. D., Tsekeris P., Lawler J. E., 1993, *A&A*, 273, 707
- Blackwell D. E., Booth A. J., Menon S. L. R., Petford A. D., 1986, *MNRAS*, 220, 289
- Blackwell D. E., Booth A. J., Menon S. L. R., Petford A. D., 1987, *A&A*, 180, 229
- Blackwell D. E., Menon S. L. R., Petford A. D., 1983, *MNRAS*, 204, 883
- Blackwell D. E., Menon S. L. R., Petford A. D., Shallis M. J., 1982, *MNRAS*, 201, 611
- Blackwell D. E., Petford A. D., Shallis M. J., Leggett S., 1982, *MNRAS*, 199, 21
- Blackwell-Whitehead R. J., Lundberg H., Nave G., Pickering J. C., Jones H. R. A., Lyubchik Y., Pavlenko Y. V., Viti S., 2006, *MNRAS*, 373, 1603
- B ohm-Vitense E., 1958, *Zeitschrift f ur Astrophysik*, 46, 108
- Bonifacio P., Spite M., Cayrel R., Hill V., Spite F., Fran ois P., Plez B., Ludwig H., Caffau E., Molaro P., Depagne E., Andersen J., Barbuy B., Beers T. C., Nordstr om B., Primas F., 2009, *A&A*, 501, 519
- Brault J., Testerman L., 1972, *Kitt Peak Solar Atlas*, Preliminary edition
- Brown J. A., Tomkin J., Lambert D. L., 1983, *ApJL*, 265, L93
- Butler K., Giddings J., 1985, *Newsletter on Analysis of Astronomical Spectra*, University of London, 9
- Canuto V. M., Mazzitelli I., 1991, *ApJ*, 370, 295
- Casagrande L., Ram irez I., Mel endez J., Bessell M., Asplund M., 2010, *A&A*, 512, A54+
- Cayrel R., Depagne E., Spite M., Hill V., Spite F., Fran ois P., Plez B., Beers T., Primas F., Andersen J., Barbuy B., Bonifacio P., Molaro P., Nordstr om B., 2004, *A&A*, 416, 1117
- Clementini G., Carretta E., Gratton R., Merighi R., Mould J. R., McCarthy J. K., 1995, *AJ*, 110, 2319
- Cohen J. G., Christlieb N., McWilliam A., Shectman S., Thompson I., Wasserburg G. J., Ivans I., Dehn M., Karlsson T., Melendez J., 2004, *ApJ*, 612, 1107
- Drawin H.-W., 1968, *Zeitschrift fur Physik*, 211, 404
- Drawin H. W., 1969, *Zeitschrift fur Physik*, 225, 483
- Dupree A. K., Hartmann L., Smith G. H., 1990, *ApJ*, 353, 623
- ESA 1997, *VizieR Online Data Catalog*, 1239, 0
- Fuhrmann K., Axer M., Gehren T., 1993, *A&A*, 271, 451
- Fuhrmann K., Pfeiffer M., Frank C., Reetz J., Gehren T., 1997, *A&A*, 323, 909
- Gangrsky Y. P., Marinova K. P., Zemlyanoi S. G., 1995, *Journal of Physics B Atomic Molecular Physics*, 28, 957
- Gehren T., Butler K., Mashonkina L., Reetz J., Shi J., 2001, *A&A*, 366, 981
- Gehren T., Korn A. J., Shi J., 2001, *A&A*, 380, 645
- Gehren T., Liang Y. C., Shi J. R., Zhang H. W. and Zhao G., 2004, *A&A*, 413, 1045
- Gehren T., Shi J. R., Zhang H. W., Zhao G., Korn A. J., 2006, *A&A*, 451, 1065
- Gratton R. G., Sneden C., 1991, *A&A*, 241, 501
- Grevesse N., Blackwell D. E., Petford A. D., 1989, *A&A*, 208, 157
- Grupp F., 2004a, *A&A*, 420, 289
- Grupp F., 2004b, *A&A*, 426, 309
- Grupp F., Kurucz R. L., Tan K., 2009, *A&A*, 503, 177
- Hauschildt P. H., Allard F., Baron E., 1999, *ApJ*, 512, 377
- Johnson J. A., 2002, *ApJS*, 139, 219
- Korn A. J., Shi J., Gehren T., 2003, *A&A*, 407, 691

- Kurucz R. L., 1992, *Revista Mexicana de Astronomia y Astrofisica*, vol. 23, p. 45
- Kurucz R. L., Furenlid I., Brault J., Testerman L., 1984, *Solar flux atlas from 296 to 1300 nm*. National Solar Observatory Atlas, Sunspot, New Mexico: National Solar Observatory, 1984
- Lai D. K., Bolte M., Johnson J. A., Lucatello S., Heger A., Woosley S. E., 2008, *ApJ*, 681, 1524
- Maltby P., Avrett E. H., Carlsson M., Kjeldseth-Moe O., Kurucz R. L., Loeser R., 1986, *ApJ*, 306, 284
- Manso Sainz R., Landi Degl'Innocenti E., 2002, *A&A*, 394, 1093
- Martin G. A., Fuhr J. R., Wiese W. L., 1988, *Atomic transition probabilities. Scandium through Manganese*. New York: American Institute of Physics and American Chemical Society, 1988
- Mashonkina L., Gehren T., Shi J., Korn A., Grupp F., 2010, in K. Cunha, M. Spite, & B. Barbuy ed., *IAU Symposium Vol. 265, Fe I/Fe II ionization equilibrium in cool stars: NLTE versus LTE*. pp 197–200
- Mashonkina L., Zhao G., Gehren T., Aoki W., Bergemann M., Noguchi K., Shi J. R., Takada-Hidai M., Zhang H. W., 2008, *A&A*, 478, 529
- Mashonkina L. J., 1996, in Adelman S. J., Kupka F., Weiss W. W., eds, *M.A.S.S., Model Atmospheres and Spectrum Synthesis Vol. 108 of Astronomical Society of the Pacific Conference Series, Accurate Collisional Cross Sections: Important Input Data in NonLTE Calculations*. p. 140
- McWilliam A., Preston G. W., Sneden C., Searle L., 1995, *AJ*, 109, 2757
- Meléndez M., Bautista M. A., Badnell N. R., 2007, *A&A*, 469, 1203
- Mihalas D., 1978, *Stellar atmospheres /2nd edition/*. San Francisco, W. H. Freeman and Co., 1978. 650 p.
- Nahar S. N., 2009, *Journal of Quantitative Spectroscopy and Radiative Transfer*, 110, 2148
- Nouri Z., Rosner S. D., Li R., Scholl T. J., Holt R. A., 2010, *Phys. Scr.*, 81, 065301
- Pickering J. C., Thorne A. P., Perez R., 2001, *ApJS*, 132, 403
- Preston G. W., Sneden C., Thompson I. B., Shtetman S. A., Burley G. S., 2006, *AJ*, 132, 85
- Reetz J. K., 1999, *Sauerstoff in kühlen Sternen und die chemische Entwicklung der Galaxis*. LMU München
- Rudolph J., Helbig V., 1982, *Journal of Physics B Atomic Molecular Physics*, 15, L599
- Ruland F., Biehl D., Holweger H., Griffin R., Griffin R., 1980, *A&A*, 92, 70
- Saloman E., 1993, *Spectrochimica Acta*, 48, 1139
- Seaton M. J., 1962, in Bates D. R., ed., *Atomic and Molecular Processes The Theory of Excitation and Ionization by Electron Impact*. p. 375
- Shchukina N., Trujillo Bueno J., 2001, *ApJ*, 550, 970
- Shchukina N. G., Trujillo Bueno J. T., 2009, in S. V. Berdyugina, K. N. Nagendra, & R. Ramelli ed., *Astronomical Society of the Pacific Conference Series Vol. 405, Three-dimensional Radiative Transfer Modeling of the Second Solar Spectrum of Titanium*. p. 275
- Shi J. R., Gehren T., Butler K., Mashonkina L. I., Zhao G., 2008, *A&A*, 486, 303
- Short C. I., Hauschildt P. H., 2005, *ApJ*, 618, 926
- Smith G. H., Churchill C. W., 1998, *MNRAS*, 297, 388
- Steenbock W., Holweger H., 1984, *A&A*, 130, 319
- Tafelmeyer M., Jablonka P., Hill V., Shetrone M., Tolstoy E., Irwin M. J., Battaglia G., Helmi A., Starkenburg E., Venn K. A., Abel T., Francois P., Kaufer A., North P., Primas F., Szeifert T., 2010, ArXiv e-prints
- van Leeuwen F., 2007, *A&A*, 474, 653
- van Regemorter H., 1962, *ApJ*, 136, 906
- Wijbenga J. W., Zwaan C., 1972, *Sol. Phys.*, 23, 265
- Yang J., Hu X., Wu H., Fan J., Cong R., Cheng Y., Ji X., Yao G., Zheng X., Cui Z., 2009, *Chinese Journal of Chemical Physics*, 22, 615

This paper has been typeset from a $\text{\TeX}/\text{\LaTeX}$ file prepared by the author.